Molecular Crystals and Liquid Crystals Incorporating Nonlinear Optics

Publication details, including instructions for authors and subscription information:
http://www.tandfonline.com/loi/gmcl17

Liquid Crystal Television

T. Uchida [a] , S. Morozumi [b] & A. Sasaki [c]

[a] Department of Electronic Engineering, Faculty of Engineering, Tohoku University, Sendai, 980, Japan

[b] Fundamental Technology Research Department, Seiko Epson Corporation, Suwa, 392, Japan

[c] Department of Electrical Engineering, Kyoto University, Kyoto, 606, Japan

Version of record first published: 03 Jan 2007.

To cite this article: T. Uchida , S. Morozumi & A. Sasaki (1988): Liquid Crystal Television, Molecular Crystals and Liquid Crystals Incorporating Nonlinear Optics, 165:1, 533-571

To link to this article: http://dx.doi.org/10.1080/00268948808082212

Mol. Cryst. Liq. Cryst., 1988, Vol. 165, pp. 533–571
Reprints available directly from the publisher
Photocopying permitted by license only

Printed in the United States of America

Liquid Crystal Television

T. UCHIDA

Department of Electronic Engineering, Faculty of Engineering, Tohoku University, Sendai, 980 Japan

and

S. MOROZUMI

Fundamental Technology Research Department, Seiko Epson Corporation, Suwa, 392 Japan

and

A. SASAKI

Department of Electrical Engineering, Kyoto University, Kyoto, 606 Japan

(Received April 11, 1988)

1. INTRODUCTION

The application of liquid crystal to display devices was first proposed by Heilmeier *et al.*[1] in 1968, and a liquid crystal television (LC-TV) addressed by electron beam was made as a trial in the same year.[2] Since then, it has taken about 15 years for practical LC-TVs to be developed. Full-color, higher resolution and greater pixel number have been attained, and presently, at least for small size LC-TVs, image quality has become very close to that of CRTs.

Two kinds of relatively high resolution LCD matrices have been developed for application to LC-TVs: the multiplexed direct-driving type and the active matrix type. Both types have been practically applied to the LC-TV, but their characteristics are rather different from each other. The former has a simple structure and low production cost, while generally the latter has a higher image quality.

General reviews on the multiplex LCD,[3,4] the active matrix LCD,[5–7]

and their applications to LC-TVs[8] are currently available. Thus, the authors review fundamental principles emphasizing gray shade, which is very important to TV displays. Finally, the actual configuration, performance and trends of the LC-TV are described.

2. FUNDAMENTALS OF LC-TVs

2.1. Multiplexed direct-driving method

2.1.1. Configuration and operation. Research on LC-TVs with multiplexed direct-driving method, which applies time-divided scanning signals to the dot-matrix liquid crystal cells, started in the '70s. The liquid crystal cell employed the twisted-nematic (TN) mode, which was proposed by Schadt and Helflich in 1971.[9] Then, the driving scheme for this LCD was established by Alto, *et al.*[10] With these works, an actual LC-TV model was developed.[11] Although image degradation caused by the increase of scanning lines is a serious problem, the multiplexed direct-driving TN-LCD has been applied to mass-produced LC-TVs with improvements in the driving scheme, LC material, and cell structure, as described below.

The multiplexed LC panel consists of two glass substrates, each of which has X- and Y-stripe electrodes, respectively, as shown in Figure 1(a). X-electrodes (scanning lines) are successively addressed by time-divided addressing pulses, and the corresponding data signals are simultaneously applied to all Y-electrodes (data lines). Figure 1(b) shows typical voltage waveform for lines X_1, X_2, and Y_1 [$V(X_1)$, $V(X_2)$ and $V(Y_1)$, respectively] and for pixels corresponding to the cross points of X_1, X_2, and Y_1 electrodes [$V(X_1,Y_1)$, $V(X_2,Y_1)$, respectively]. In order to maintain the stability of the liquid crystal, polarity of the scanning and data voltages is reversed at half period of one scanning line. Gray scale is generated by equally divided pulse widths of the data signals in the scanning period of one line as shown in the middle part of Figure 1(b).

The driving waveforms are optimized by maximizing the ratio of rms-voltages applied to pixels of highest to lowest brightness, V_h/V_l. The optimized ratio V_h/V_l is expressed as a function of scanning line numbers N as follows:

$$V_h/V_l = \{(N^{1/2} + 1)/(N^{1/2} - 1)\}^{1/2}. \quad (1)$$

The equation indicates that V_h/V_l decreases and approaches to unity as N increases. Therefore, a display mode with steep threshold prop-

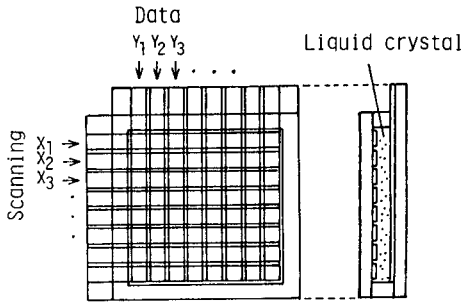

(a) Structure of multiplexed LCD

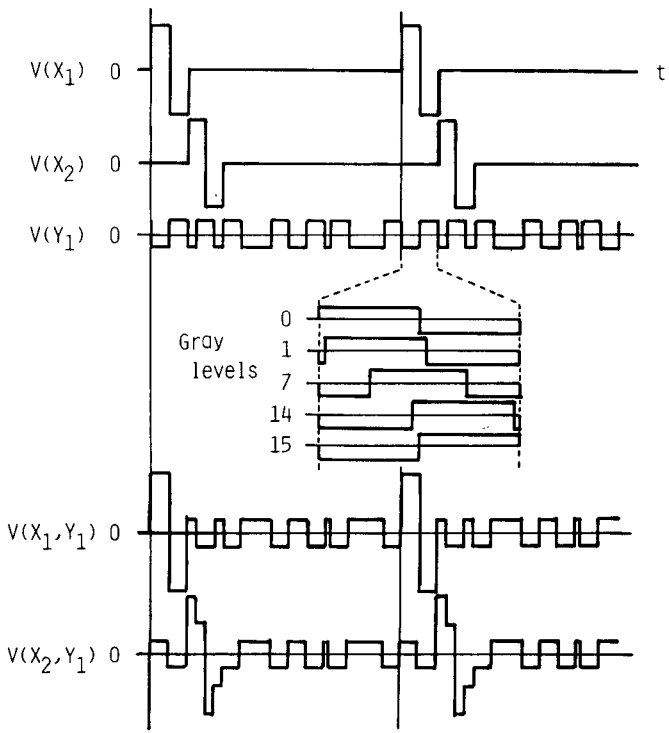

(b) Driving voltage waveform

FIGURE 1 Structure and waveform of the multiplexed LCD.

erties in the voltage-transmission curve is required. For such a display mode, twisted-nematic (TN) cells have been used and the effects of various parameters have been analyzed and optimized. Among these parameters, the most important one is the ratio of bend and splay elastic constants, K_{33}/K_{11}.[12-16] Many efforts have been made to decrease it, and at present a value of around 0.65 has been achieved. However, the number of scanning lines is still limited to about 60 if satisfying contrast and viewing angles are required. The typical characteristics will be mentioned in Section 3.1.

2.1.2. Improvement of image quality. In order to improve image quality by increasing the duty ratio, double-matrix[17] (or quad-matrix[18]) and overlap-addressing method have been developed. The matrix structure and the addressing voltage waveform are shown in Figures 2 and 3, respectively. The double-matrix method increases duty ratio twice without a decrease of vertical pixel number. However, it has the following disadvantages:

—The edge of each *Y*-electrode (ITO) must be coated with thin metal to decrease the resistance of the narrow parts of the *Y*-electrodes.

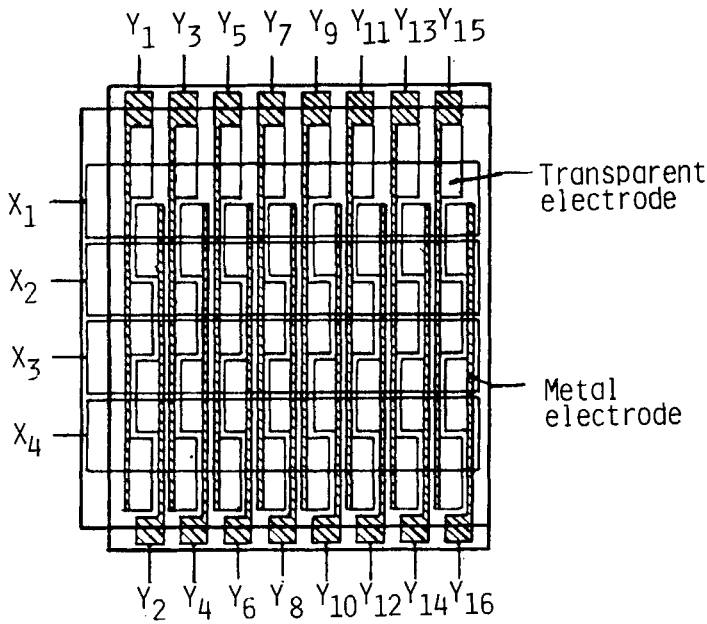

FIGURE 2 Double matrix LCD.

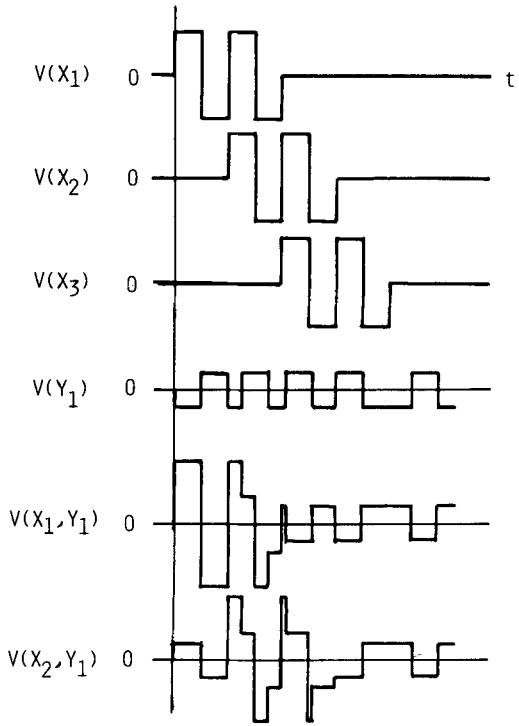

FIGURE 3 Overlapping addressing method.

—It requires twice the number of *Y*-electrode connections and circuits.

—Aperture ratio becomes small.

The overlap-addressing method also increases the duty ratio twice without reducing the number of scanning lines as shown in Figure 3. The assigned period for each scanning line is doubled and half of it is overlapped with the next line.[19] Therefore, the brightness level becomes the average of two adjacent pixels of the original image, and hence the resolution itself decreases to one half, while the smoothness of halftone image is much better than a conventional LCD. It is clearly effective to improve image quality.

Image quality can be also improved by increasing threshold steepness. The threshold becomes steeper as the twist angle of the molecular alignment in the TN-cell increases. Cells with a twist angle greater than 90° are called super-twisted nematic cell (STN-cell),[20] and in particular the super-twisted cells utilizing birefringence effect

are called super-twisted birefringent cell (SBE-cell).[21] The STN-cell has a twist angle of generally around 120°–240° and pretilt angle of around 0.5–5°, while the SBE-cell has a twist angle of around 270°, and a pretilt angle of around 20°. However, the original STN-cell and SBE-cell have the drawbacks of yellow background color and slow response, so that they are not suitable for black/white LC-TVs or the full-color LC-TV mentioned later. Several methods have been proposed to remove the background color. One of them is the optical mode interference cell (OMI-cell)[22] or black and white STN-cell (B/W-STN-cell),[23] in which product of birefringence and cell gap, Δnd, and directions of two polarizers are suitably adjusted. The other is the compensated STN-cell, which is composed of two complementary STN-cells with the same Δnd, but opposite twist directions,[24] and exhibits excellent contrast. However, as far as the multiplexed LCDs are concerned, the tradeoff between scanning line number and response speed still remains to be solved, and some break-through is necessary to overcome it.

2.2. Active matrix method

One solution to the problem of the limitation in scanning line number and response time in the multiplexed direct-driving LCD is the active matrix method. The first idea of an active matrix addressing scheme, in which transistors or diodes are arranged at each pixel to store the charge, was proposed by Lechner *et al.*[25,26] Since then, development of active matrix LCDs started with cadmium-selenide (CdSe) TFTs which had previously been researched for electronic devices[27,28] such as image sensor scanner circuits. In the early '70's, actual display panels with CdSe TFT array were fabricated by Brody, *et al.*[29,30] and by Lipton and Koda,[31] and successive works[32–34] have been continued. Although CdSe TFTs have excellent carrier mobility and are easily fabricated by evaporation, because of their toxicity and instability problems, they are not yet in commercial use.

MOS transistor array on silicon single crystal wafer[35] and SOS (silicon on sapphire) substrate,[36] and TFTs with tellurium (Te)[37] were developed in substitution for CdSe TFTs. In particular, the MOS array was applied to active matrix LC-TVs,[38,39] but they were not successful. Since the late '70's, with the appearance of amorphous silicon film,[40] active matrix technology advanced and was put in practical use. At the same time, the research on polycrystallized silicon TFT contributed to this advance, resulting in the first successful production of practical small-sized LC-TV[41] with full color capability.

At present, silicon TFTs on glass substrate have become a major approach to active matrix liquid-crystal (LC) TV displays.[42]

Aside from such transistor-type active matrix LC display, diode elements have been researched since the late '70's with zinc-oxide (ZnO) substrates[43] and metal–insulator–metal (MIM) thin film diodes on glass.[44] Then, LCDs with amorphous silicon ring diodes[45] and back-to-back diodes[46] were developed. Since diodes can be fabricated more easily than TFTs, developmental efforts of diode-type active matrix technology resulted in LC-TVs with MIM[47] and amorphous silicon pn diodes[48] as well as those with TFTs.

In this section, the fundamental driving scheme of the TFT-matrix and the diode-matrix LCDs is described, and the actual LC-TVs with active matrix method are discussed later in Sections 3.2 and 3.3.

2.2.1. Thin-film transistor (TFT) type. A basic active matrix LCD using TFT array is shown in Figure 4. The required ON current I_{ON} and OFF current I_{OFF}, which are drain currents when the gate is opened and closed, by suitable gate voltages, respectively, are roughly estimated as follows. When T_f denotes frame time, N scanning line number, V_d highest voltage applied to drain as shown in Figure 5 by the solid line, C_L capacitance of liquid crystal for one pixel, I_{ON} must satisfy the following inequality to charge up the pixel capacitor in a scanning period:

$$I_{ON} \geqq C_L V_d \, N/T_f \tag{2}$$

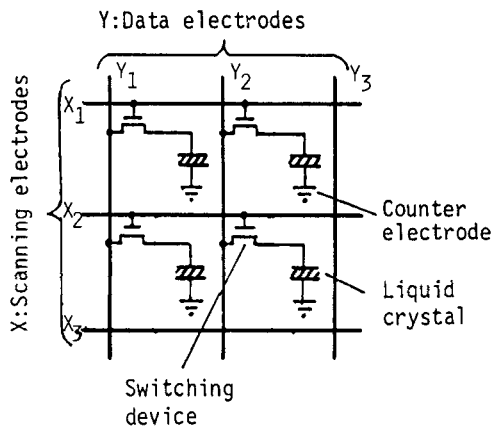

FIGURE 4 TFT type active matrix LCD.

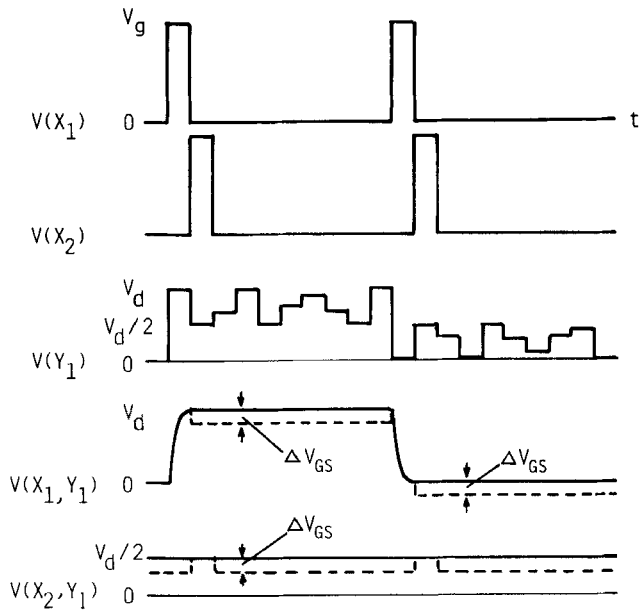

FIGURE 5 Voltage waveform applied to the TFT type matrix LCD. $V(X_n)$; gate voltage, $V(Y_n)$; drain voltage, $V(X_n, Y_n)$; pixel voltage. Solid line; ideal case, Broken line; actual case affected by the parasitic capacitor C_{GS}.

I_{OFF} is given by the condition that the change of pixel voltage must be smaller than a given value ΔV, that is,

$$I_{OFF} \leqq C_L \Delta V / T_f \tag{3}$$

Here, if the leakage current I_L through the liquid crystal resistance R_L is taken into account and the current is assumed to be small enough, the following inequality must be satisfied:

$$I_L + I_{OFF} \approx V_p / R_L + I_{OFF} \leqq C_L \Delta V / T_f \tag{4}$$

where V_p ($V_l \leqq V_p \leqq V_h$) is a voltage applied to the pixel. As a typical example, if the area of one pixel S_p is assumed to be 200 μm × 200 μm, d = 6 μm, C_L = 0.4 pF, T_f = 1/60 sec, $\mathbf{V_d/z} = V_p = 3V_{th}$ = 6V (Vth denotes optical threshold voltage of liquid-crystal), $\Delta V = V_{th}/10$ = 0.2V, N = 240, then I_{ON}, I_{OFF} and I_{ON}/I_{OFF} become

$$I_{ON} \geqq 6.9 \times 10^{-8}(A), \tag{5}$$

$$I_L + I_{OFF} \leqq 4.8 \times 10^{-12}(A), \tag{6}$$

$$I_{ON}/(I_L + I_{OFF}) \geqq 1.4 \times 10^4. \tag{7}$$

From inequality (6), the resistivity of the liquid crystal material, ρ_L, must satisfy the following inequality:

$$\rho_L \geqq \frac{V_p S_p T_f}{d\, C_L\, \Delta V} = 8.3 \times 10^{11} \quad \text{(ohm-cm)}. \tag{8}$$

Therefore, the liquid crystal resistivity must satisfy rather severe condition.

If inequality (3) is satisfied but inequality (4) or (8) is not, the problem can be solved by increasing V_p to obtain the desired rms-voltage as long as ρ_L is constant over the whole area of the LC panel. However, if inequality (3) is not satisfied, the increase of V_p as mentioned above is not sufficient, because the values of I_{OFF} in the odd and even frame are generally different; this causes flicker. One solution to this problem is to alternate the polarity of the pixel voltage row by row and column by column to average out flicker.[49]

The more reliable but costly method is to add a storage capacitance C_s to each individual pixel. In this case, C_L in inequalities (2–4) and (8) is replaced by $C_L + C_s$, and hence the required I_{OFF} and ρ_L conditions become less severe.

The TFT-active matrix presents crosstalk problem because of the parasitic capacitance between source and drain, C_{SD}, and between gate and source, C_{GS}. The former is due to the overlap among light shield metal, source and drain, and planar coupling between pixel and drain bus.[50] However, these values are much smaller than the pixel capacitance, so that they can be neglected. On the other hand, C_{GS} has been clarified not only due to the overlap between gate and drain but also to returning carriers to the channel with the switching-off of the gate voltage.[51] Therefore, C_{GS} cannot be decreased to one half of the gate capacitance even if the overlap between gate and source is removed.[50] Because of the effect of C_{GS}, the actual voltage applied to a pixel $V(X_1,Y_1)$ or $V(X_2,Y_1)$ becomes as shown in Figure 5 by the broken line instead of the solid line. The voltage shift ΔV_{GS} due to C_{GS} is given by

$$\Delta V_{GS} = V_G C_{GS}/(C_{GS} + C_L). \tag{9}$$

Then, if C_{GS} is constant over the whole area of the panel, ΔV_{GS} is constant, so that this voltage shift can be canceled by shifting the voltage of the counter electrode from $V_d/2$ to $V_d/2 - \Delta V_{GS}$. Addition of a storage capacitor to each pixel is also effective to decrease ΔV_{GS} and then to relax the condition of C_{GS} uniformity.

2.2.2. Diode type. Configuration and general driving waveform of the diode matrix are shown in Figures 6 and 7. Since this type basically consists of a non-linear device and capacitance, its behavior becomes more complicated than that of the TFT-type. For the first step of analysis, resistance of the liquid crystal is neglected. Here, voltage across the diode at the end of the scanning period is assumed to be V_{D2} and that in the storage period to be V_{D1} as shown in Figure 8, where the diode current $I(V_{D1})$ is sufficiently small to discharge the stored voltage of pixels.

The voltages applied to the pixels for the highest and the lowest brightness, V_h and V_l, respectively, are written by the scanning pulse V_s and highest data signal voltage $\pm V_c$ shown in Figure 7 as follows:

$$V_h = V_s + V_c - V_{D2} \quad (\geqq 0) \tag{10}$$

$$V_l = V_s - V_c - V_{D2} \quad (\geqq 0) \tag{11}$$

These equations can be rewritten for the expression of V_c and V_s as

$$V_c = (V_h - V_l)/2 \tag{12}$$

$$V_s = (V_h + V_l)/2 + V_{D2} \tag{13}$$

On the other hand, the storage condition of the pixel voltage in the stored period are expressed as follows:

$$V_h - (V_b - V_c) \leqq V_{D1} \tag{14}$$

$$V_b + V_c - V_l \leqq V_{D1} \tag{15}$$

From equations and inequalities (12–15), the following inequalities are obtained.

$$3(V_H - V_l)/2 - V_{D1} \leqq V_b \leqq (V_h - 3V_l)/2 + V_{D1} \tag{16}$$

$$V_h - V_l \leqq V_{D1} \tag{17}$$

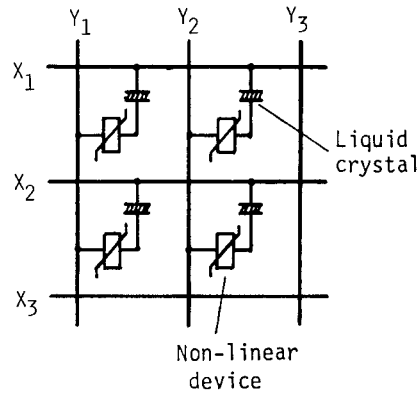

FIGURE 6 Diode type active matrix LCD.

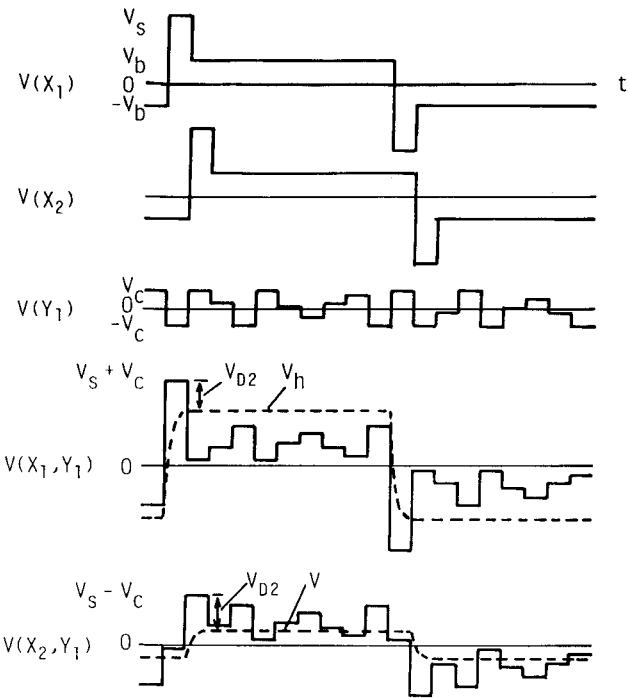

FIGURE 7 Voltage waveform applied to the diode type matrix LCD. $V(X_n)$; scanning voltage, $V(Y_n)$; data voltage, $V(X_n, Y_n)$; pixel voltage.

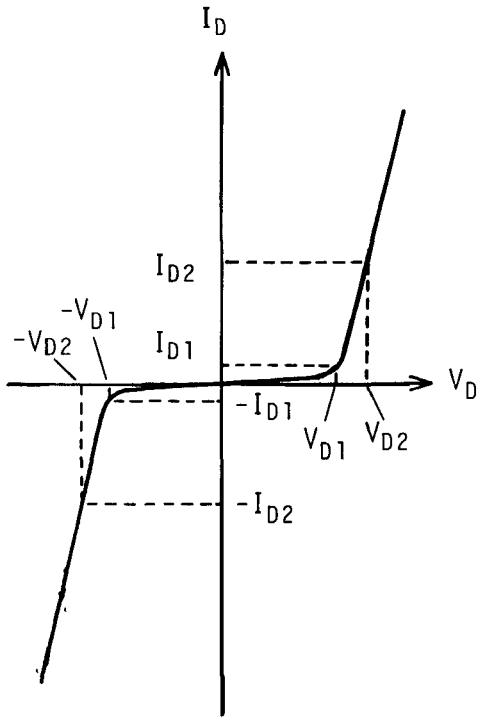

FIGURE 8. Voltage-current property of diode.

Here, if the threshold voltage of LCD is expressed by V_{th}, the desirable condition is given by

$$V_l \leqq V_{th} \quad \text{and} \quad V_h \geqq 3V_{th}. \tag{18}$$

From inequality (17) and (18), $V_{D1} \geqq 2V_{th}$ is obtained as a desirable condition for the diode.

For diodes with low V_{D1} such as ring diode,[45] $V_h - V_l$ is chosen to be equal to V_{D1} to maximize it from inequality (17). Then, from equations and inequalities (12–15), V_c, V_b, and V_s become as follows:

$$V_c = V_{D1}/2 = V_h - V_l/2 \tag{19}$$

$$V_b = (V_h + V_l)/2 \tag{20}$$

$$V_s = (V_h + V_l)/2 + V_{D2} = V_b + V_{D2} \tag{21}$$

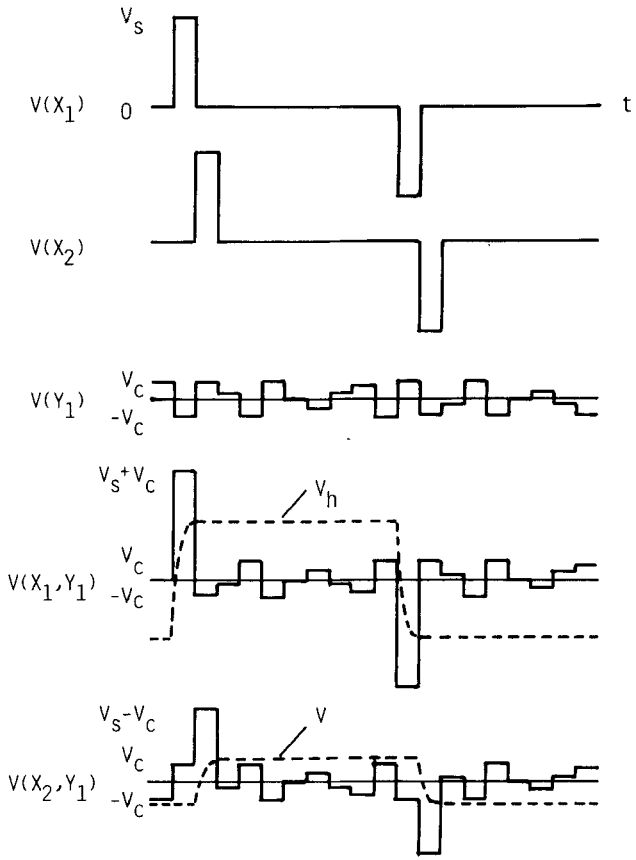

FIGURE 9 Voltage waveform for the diode with low V_{D2}.

The voltage waveform in this case is shown in Figure 9. It should be noticed that a diode with insufficient non-linearity has a high V_{D2}, which means that a high V_s is required.

On the other hand, in the case of diodes with high V_{D1} such as Z_nO varistor[43] and back-to-back diode,[46] inequality (14) satisfies inequalities (15) as well as (17), if $2V_b \leqq V_h + V_l$ is assumed. Therefore V_b can be taken to be zero for simplicity. Substituting $V_b = 0$ and inequality (12) into inequality (14), we obtain the following inequality:

$$V_h \leqq (2V_{D1} + V_l)/3 \tag{22}$$

Therefore, the maximum value of V_h becomes $(2V_{D1} + V_1)/3$. Substituting this V_h into inequalities (12) and (13) gives:

$$V_c = (V_{D1} - V_l)/2 \tag{23}$$

$$V_s = ((V_{D1} - - 2V_l)/3 + V_{D2} \tag{24}$$

The applied voltage waveforms are shown in Figure 10. If V_l is taken to be V_{th}, V_h is lower than that in the former case by a factor of $(2V_{D1} + V_{th})/3(V_{D1} + V_{th})$.

In the case of an insufficiently non-linear diode such as MIM-diode,[52,53] V_{D1} is rather small. Therefore, instead of V_{D1}, a suitable value V_{D1}, larger than V_{D1} is sometimes adopted at the sacrifice of storage. Namely, the discharge current from the pixel becomes non-negligible and is affected by the displayed pattern of the other pixels on the same column. This problem can be solved by exchanging the polarity of the voltages row by row (or every two rows), which averages the discharge condition of each pixel.

The general problem of the diode matrix is a relatively larger parasitic capacitance between the pixel and data line as compared to the TFT. Because of this capacitance, the voltage stored in the nth pixel deviates by $-\{V_s + V_c - V_b + V_p(n + 1)\} C_D/(C_L + C_D)$, where $V_p(n + 1)$ ($|V_p(n + 1)| \leqq V_c$) is the voltage applied to $(n + 1)$th pixel. Here, the first three terms of the deviation can be canceled by suitably shifting the waveform because they are constant, while the last term cannot. In order to solve this problem, C_D must be decreased or a storage capacitor C_S must be added to C_L. From another point of view, however, the last term can be positively utilized as an edge enhancement if the polarity of pixel voltage is exchanged row by row.

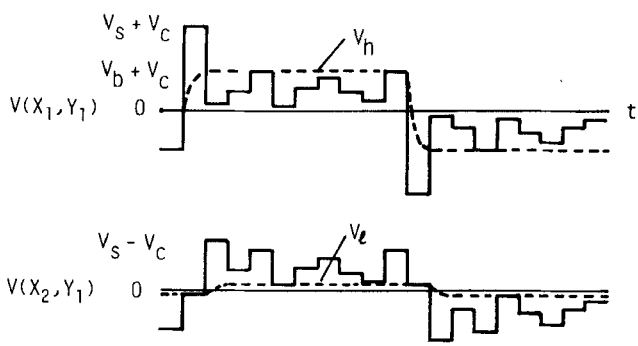

FIGURE 10 Voltage waveform for the diode with high V_{D2}.

2.2.3. Liquid crystal mode suitable for active matrix LCDs. The active matrix driving does not need the steep threshold as required to the multiplexed drive mentioned before. Contrast and viewing angle are very important for an image quality in the active matrix LCDs.

The mode mostly used in the active matrix system is the normally-black-TN-mode with parallel polarizers. Contrast of this mode is determined mainly by the blackness in the off-state. Figure 11 shows the transmittance of this mode at the off-state as a function of $\Delta nd/\lambda$ where Δn is birefringence, d is cell gap and λ is wavelength.[54] Usually, the second minimum condition, with $\Delta nd/\lambda \geqq 1$, was chosen. However, the first minimum condition, with $\Delta nd/\lambda = \sqrt{3}/2$, has recently attracted special interest to obtain a wide viewing angle. This condition requires an accurate control of cell-gap d, because transmittance increases greatly with small deviations of $\Delta nd/\lambda$ from the optimal value. Moreover, in the case of a full-color LCD using the micro-color-filter mentioned later, λ changes among red, green and blue pixels, so that d is adjusted to obtain the optimum $\Delta nd/\lambda$ as shown in Figure 12. This is called multi-gap system.[55] This method gives ideal blackness, but very high technology is required to control the cell-gap accurately during production.

One of the solutions to the above mentioned difficulty is the normally-white-TN-mode with crossed polarizers.[56,57] Since the black level is obtained by application of high voltage, $\Delta nd/\lambda$ does not have to be strictly controlled. However, a relatively high voltage is required to obtain a sufficient black state, and hence additional measures must be taken to assure the stability of the TFT.

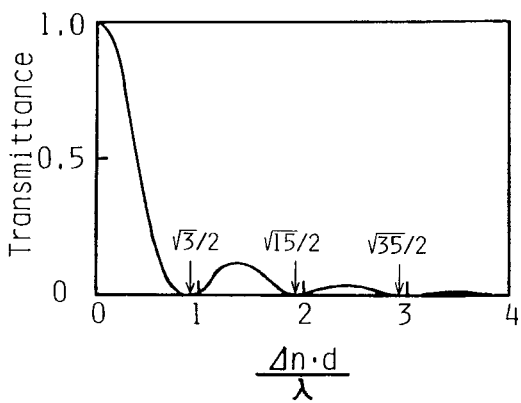

FIGURE 11 Transmittance of the normally-black-TN-cell as a function of $\Delta nd/\lambda$.

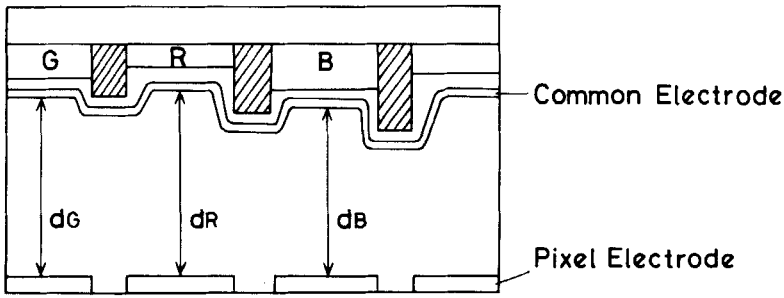

FIGURE 12 Multigap configuration of TN-cell. The cell gaps between the common electrode and the pixel electrode are adjusted by varying the thickness of the color filter.

Another solution is Heilmeier's type guest–host mode (GH-mode)[58] doped with black dye mixture. Advantages of this method are a wide viewing angle, high blackness and a moderate steepness of threshold, suitable for gray shades. Its disadvantage is that a high voltage (about twice that of TN-mode) is necessary to obtain a sufficient white level, so a higher TFT stability is required.

The third solution is the deformation of vertically aligned mode (DAP-mode),[59] which uses nematic liquid crystal with negative dielectric anisotropy. The advantage of this mode is excellent blackness for all visible wavelengths at the off-state because of the homeotropic alignment and crossed polarizers.

2.3. Full color LCD

There are several methods to realize color LCD as shown in Figure 13, and the most practical one is the additive mixing system using micro-color filters. The idea of the micro-color filter type was proposed by Fischer, *et al.*,[66] but the filter was located outside the LCD and therefore special optics such as light parallelizer and diffuser were required. The practical idea with the color filter inside the LCD was proposed by Uchida, *et al.*[62,63] and a prototype full color LCD was demonstrated. Then, a full color LC-TV using the micro-color filter combined with TFT-type active matrix was developed and presented by Morozumi, *et al.*[41]

Generally, the color layer is placed under the counter electrode in the case of the active matrix LCD, while it is placed on the electrode in the case of the multiplexed LCD as shown in Figure 14. There are several methods for fabricating the color layer as shown in Table I. Among them, the dyeing method is most widely used at present.

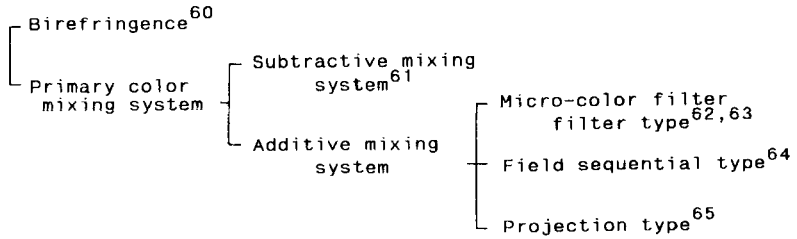

FIGURE 13 Various systems of color LCDs.

However, other methods are also being actively investigated to simplify the fabrication process.

Another promising liquid crystal color display is the projection type with additive mixing system.[65] This type is composed of three liquid-crystal light valves with red, green, and blue filters. The images of the light valves are projected and superimposed on the screen. Details and actual examples are described in Section 3.4.

3. CONFIGURATION AND ACTUAL PERFORMANCE OF LC-TV

3.1. Multiplexed LC-TV

An example of configuration of the multiplexed color LC-TV is shown in Figure 15. The color filter layer is fabricated inside the cell on

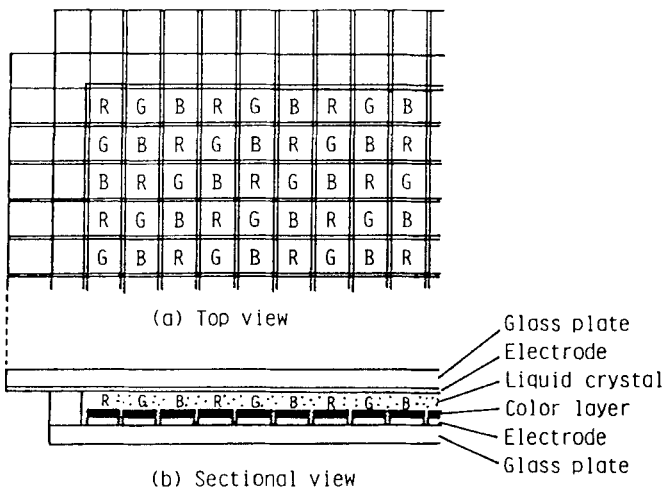

FIGURE 14 Full-color LCD with micro-color filters inside of the cell.

TABLE I

Fabrication method of color filters and their characteristics

Method	Advantage	Disadvantage
Dying [63] (Gelatin)	—Capability of high resolution	—Expensive
Electro deposition[67]	—Automatic patterning —Good uniformity in thickness	—Large voltage drop due to thick color layer
Printing[62,68]	—Low cost	—Difficulty of obtaining uniform thickness —Difficulty in alignment
Dyed photo-sensitive polymer[69,70]	—Capability of high resolution	—Under development

either the upper or lower substrate for the generation of a color image. The X driver array supplies scanning pulses synchronized with the horizontal synchronizing signal on the video composite video signal. The Y driver connected to the Y electrodes has input terminals for receiving the clock and 4-bit digitized R, G, and B video signals. The pulse-width modulators inside the Y driver generate 16 kinds of pulse

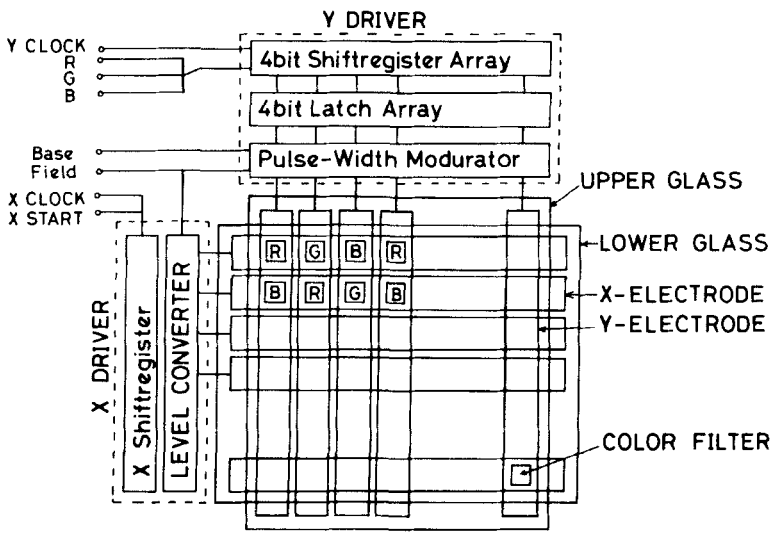

FIGURE 15 Configuration of video display with highly multiplexed direct-driving twisted-nematic liquid crystal display (TN-LCD).

periods corresponding to the desired gray levels as shown in Figure 1. Usually, ¼ or ½ of the effective number of scanning lines is applied to small size video display, that is around 120 or 240 in the case of NTSC (National Television System Committee) system. Since the multiplexed direct-driving method has serious image degradation problems when the number of scanning lines is increased, as described in Section 2.1.1., the multiplexing duty ratio is halved by driving the divided Y electrodes into upper and lower regions from both sides of the screen with double Y driver circuits; otherwise overlapped-addressing method is employed as mentioned in Section 2.1.2.

The image performance of highly multiplexed TN-LCDs is relatively inferior to that of the active matrix LCD, but with recent considerable efforts towards improvements, an acceptable image quality was realized. For example, a peak contrast ratio over 20:1 was obtained at a duty ratio of 1/55 with a directly multiplexed TN-LCD cell incorporated into color LC-TV, with 109 (V) × 480 (H) pixels in an area of 2.5″ diagonal. In this LCD, the overlapped-addressing method[19] was employed and the ITO electrodes were fabricated on the color filter layer in order to improve the contrast ratio. The viewing angle ranges are presumed to be 5° and 15° for the upper and lower direction and 40° for left and right, respectively, over a contrast ratio of 8:1, in which the viewing angle range for the upper and lower direction is particularly narrow. A photograph of a color pocket LC-TV set incorporating the multiplexed direct-driving LC display is shown in Figure 16. External dimensions are 85 mm × 145 mm with a thickness of 26 mm, with 4 pieces of unit 3 batteries included.

3.2. Active matrix LC-TV with TFT arrays

Active-matrix liquid-crystal display technology with thin-film transistor (TFT) arrays is an approach allowing a high quality video image. As mentioned in Section 2.2, the development of active matrix liquid-crystal technology started with Lechner, *et al.*'s suggestion and cadmium-selenide (CdSe) TFTs. However, today most efforts towards TFT type active matrix LCDs have shifted to amorphous silicon (a-Si) and polycrystallized silicon (poly-Si) TFTs. Among various TFT-LCDs, typical examples of silicon film for full color liquid crystal TV displays will be mentioned below.

3.2.1. Full color TFT-LCD with a-SI TFT array. The history of a-Si TFTs began in 1975 with the employment of hydrogen doping into a-Si film[40] to discriminate the p and n type films in their fabri-

FIGURE 16 Photograph of TV set with 2.5″ full color multiplexed TN-LCD.

cation. These methods have stimulated the investigation of TFT characteristics. Since the late '70's, many attempts[71–73] have been made to fabricate TFTs with a-Si film and to apply them to active matrix LCDs. Due to the extremely high resistivity in the OFF condition, a-Si TFTs have an excellent ON/OFF current ratio: as high as 10^6 in spite of the low ON current determined by a small carrier mobility. However, they had serious problems in electrical stability[74] in that the current was easily altered with the applied voltage. After a long time this was solved with the use of continuous deposition of silicon nitride film as a gate insulator and a-Si film without breaking the vacuum condition.[75] Thus, at present, the a-Si TFT has become a major device to realize active matrix LCDs.

Various structures and fabrication processes of a-Si TFTs have been developed,[76–78] with similar electrical characteristics: the resistivity under dark condition is 10^{14} ohm-cm, the electron mobility in the inverted channel surface is 0.1–1.0 $cm^2/V \cdot sec$, and the threshold voltage is 2–5 volts. Most a-Si TFTs employ the inverted staggered structure, in which nondoped a-Si layer is deposited over silicon nitride gate insulator on metal gate electrode, with n^+ a-Si and metal layers for ohmic contact in the source and drain electrodes. The gate insulator and a-Si layer are continuously deposited in the plasma enhanced chemical-vapour-deposition (P-CVD) furnace in which silane (SiH_4) gas is decomposed.

The cross sectional view of the typical LCD panel with a-Si TFT array[75] is illustrated in Figure 17. The a-Si TFT and associated pixel electrode with additional capacitor electrode are formed on the lower glass substrate. On the opposite substrate, the color filter layer for comprising the color pixel aligned to the driving electrode, and black grid area to shield the light passing through the gaps between the pixel electrodes are fabricated. The elements on the lower substrate are fabricated as follows: First, before the fabrication of the TFT, the ITO layer for the additional pixel capacitor electrode is formed, and SiO_2 film is deposited. Next, the ITO pixel electrodes are formed on the SiO_2 film before the fabrication of the TFT array. Gate electrodes and contacting layer between ITO pixel electrode and aluminum layer made of chromium, are formed. Then, the first silicon nitride film for the gate insulator, a-Si layer, and the second silicon nitride film for passivation over the TFT channel, are continuously deposited by P-CVD method. After forming the pattern of the second silicon nitride layer, the ohmic-contact layer consisting of phosphorous doped a-Si film for the source and drain electrode is deposited and patterned. After opening the through-holes between the ITO pixel electrode and drain electrodes, the double metal layer of molybdenum and aluminum for the metallization from source and drain electrodes is fabricated. These elements on this substrate are completed with 9 photomask layers.

The electrical characteristics of this a-Si TFT with channel width to length ratio of W/L = 20 are shown in Figure 18. The mobility is

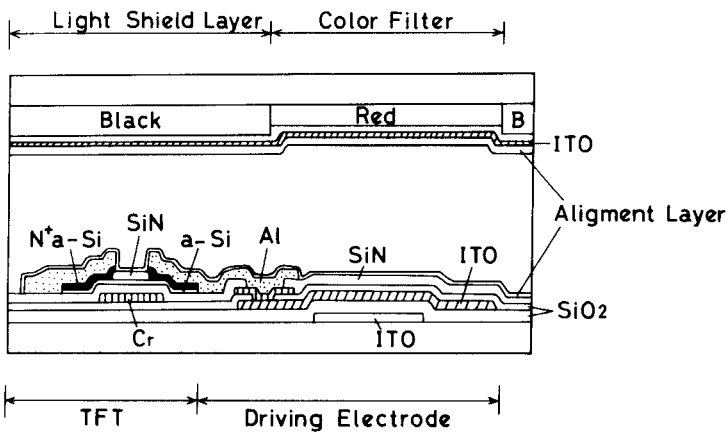

FIGURE 17 Cross-sectional view of full color active matrix LCD with amorphous silicon TFT array.

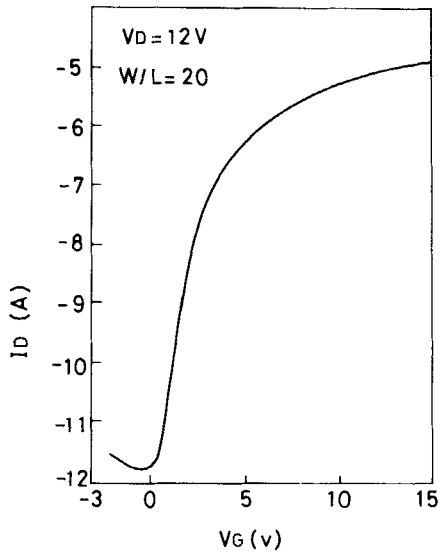

FIGURE 18 Characteristics of amorphous silicon thin-film transistor (TFT).

calculated as 0.9 $cm^2/V \cdot sec$, and the threshold voltage is 2.5 volts. If the liquid crystal capacitance at each pixel is 0.2 pF and additional pixel capacitance is 1.0 pF, these values may assure a sufficient time constant as discussed in Section 2.2.1, for example in the case of NTSC system, 60 μsec for writing and over 16 msec for storing. The high photoconductivity under sunlight of a-Si TFT is a serious problem. The incident light from the upper substrate may be shielded by a light shield layer made of black dye. The photoconductivity of a-Si TFT can also be reduced by the employment of thin a-Si film (150–200 Å), so as to be usable under 200,000 lux of illumination, equivalent to sunlight.

In this LCD, the polarizers on both outer sides of the glass substrates are placed in parallel (normally-black mode). In order to obtain a wide viewing angle and high contrast ratio, the first minimum condition in transmittance is adopted by using multigap method[55] as mentioned in Section 2.2.3.

Among several driving schemes for the video display with gray levels, the "line-at-a-time" method, which drives each data line connected TFT row on the addressed gate line, is employed. This method is quite useful for high resolution displays. Usually, the resolution of the image on the video display is limited by two factors: one is numbers of pixels and the other is the video signal bandwidth limited by

MOS analog circuits in the column driver. The "line-at-a-time" method is suitable to obtain high speed operation to realize a wide video signal bandwidth, Figure 19 shows the circuit configuration of the "line-at-a-time" column driver. Total circuits consist of a shift register array for supplying the successive sampling pulses, analog sampler and holder array for sampling the video signal controlled by the successive sampling pulse, and analog line memory for transferring the sampled video signal from sampler and holder array to the column lines. Since the addressed pixels are driven through TFTs during the full period assigned to one scanning line, the video signal can be perfectly transferred to the pixel liquid crystal compared to the "point-at-a-time" method discussed in Section 3.2.2. Speed of the sampler and holder array limits the signal bandwidth, but when these circuits are integrated on CMOS-LSI chips, a bandwidth of more than 5 MHz can be achieved, which is an adequate value for the video display.

A 3" full color liquid crystal video display with 240 (V) × 378 (H) pixels in a 45.6 mm × 60.4 mm display area with the above mentioned a-Si TFT array has been achieved. The photograph of the pocket-sized TV incorporating this LCD is shown in Figure 20. The maximum contrast ratio is 55:1; the viewing angle for right/left is 35°, and for up/down it is 30°. The image chromaticity on this display panel was fairly close to that of CRTs.

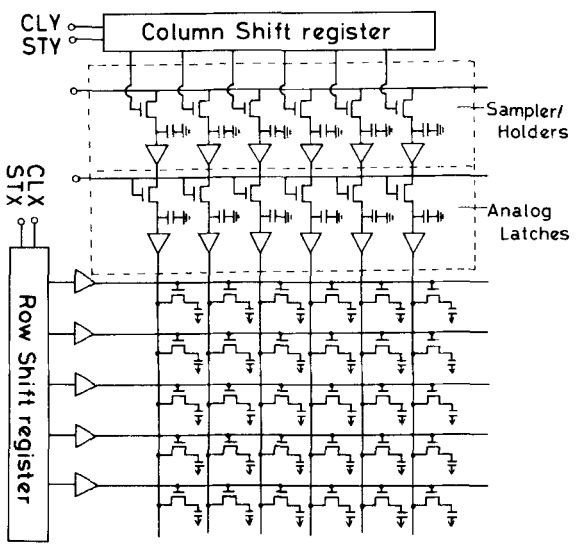

FIGURE 19 "Line-at-a-time" Driving scheme for TFT-LCD.

FIGURE 20 Photograph of full color TV set with 3" a-Si TFT-LCD.

3.2.2. Full color LC-TV with poly-Si TFT array. Properties of polycrystalline-silicon (poly-Si) film have been investigated[79] as a gate material for MOS transistor on Si single crystal wafer. Here, the low pressure and temperature chemical vapour deposition (LPT-CVD) method has been employed for the deposition of a poly-Si thin-film, in which the poly-Si layer is deposited by the thermal decomposition of the silane (SiH_4) gas at around 600°C.

In the fabrication of poly-Si TFT, two approaches are taken: one is high-temperature process[80,81] and the other is low temperature process.[82-84] The former employs a silicon oxide film as gate insulator thermally grown at over 800°C on mostly quartz substrates. The latter employs a deposited silicon oxide film formed by thermal CVD at around 450°C on hard glass, such as Corning 7059. The TFT processed at high temperature exhibits an excellent stability due to minimization of the state density at the interface between the poly-Si/gate oxide film and the area inside this oxide film. On the other hand, the stability of low temperature processed TFT is slightly less than for the high temperature one. However, with the cleaning process taking place before the careful deposition of the oxide film, a sufficient reliability[82] has been achieved.

The structure of high temperature processed TFT is shown in Figure 21(a). First, 1,500 Å thick poly-Si film is deposited by LPT-CVD at 600°C, and then the undesired area, except for the transistor region, is etched off. Following this, the 1,500 Å thick silicon oxide film for the gate insulator is grown in an oxygen atmosphere at 900–1,000°C.

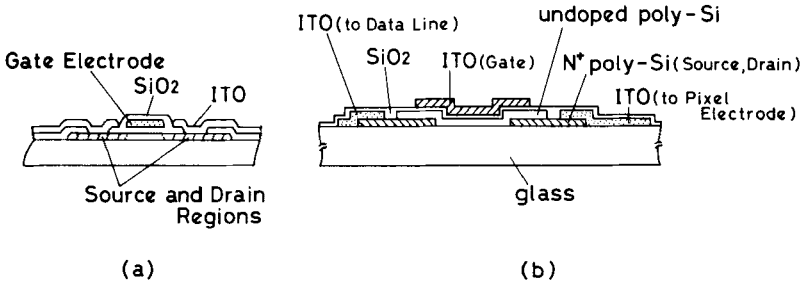

FIGURE 21 Cross-sectional view of polycrystalline silicon TFT. (a) Structure for high temperature fabrication (b) Structure for low temperature fabrication.

Here, the thickness of the remaining poly-Si film may be 750 Å. Next, poly-Si for the gate electrode is deposited again, in the same way as for the first poly-Si layer, and the gate electrode is patterned. Phosphorous ions are implanted in the gate electrode and source/drain region to form a low resistance layer and to form an ohmic contact with the external conductors, shielding the poly-Si channel region below the gate electrode from the phosphorous ions. An 8,000–10,000 Å thick silicon oxide film is deposited by thermal CVD, as an interlayer to insulate the metal conductor layer from the transistor, and then contact holes are opened. Finally, the indium–tin–oxide (ITO) layer for the data line and the pixel electrode is formed. This process is completed with four photomasks. With the employment of the ion-implanted self-alignment TFT, the parasitic capacitance at the pixel can be minimized due to the reduced overlap between the source/drain and the gate electrodes.

The structure of the low temperature poly-Si TFT is illustrated in Figure 21(b). 1,500 Å thick n^+ islands for the source and drain electrode are formed with the LPT-CVD deposition at 600°C on the glass substrate. Then, a 100–500 Å thick undoped poly-Si film is deposited by LPT-CVD, and the channel region is formed. A 200 Å ITO layer is sputtered and patterned to form the pixel electrodes and data lines. After the cleaning treatment of the semiconductor surface, the silicon oxide film for the gate insulator is deposited by CVD. Finally, the gate electrode made of metal layer is formed. This process also takes place with four photomasks. With this structure, poly-Si film thickness can be lowered below the high temperature processed one because the poly-Si film for the channel material does not have thickness reduction as exhibited by a TFT with thermally grown gate oxide film. This results in a much higher ON/OFF ratio. As with other

methods for low temperature deposition of poly-Si film, molecular beam deposition[83] and electron beam deposition[84] have been developed. In those methods similar TFT characteristics have been obtained.

The electrical characteristics of the poly-Si film are determined by traps located at the grain boundary. The trap density may affect the carrier mobility and threshold voltage of poly-Si TFT. Such traps are stable because the grain property rarely changes at room temperature, so the reliability of poly-Si TFT is sufficiently good. The actual electrical characteristics are shown in Figure 22. The ON current for both high and low temperature processed TFTs is about the same. However, since the low temperature TFT can utilize a very thin poly-Si film, it exhibits a lower OFF current than high temperature processed TFT. The mobility and threshold voltage in both TFTs are 10 cm^2/V:sec and 5 volts, respectively. In order to reduce the OFF leakage

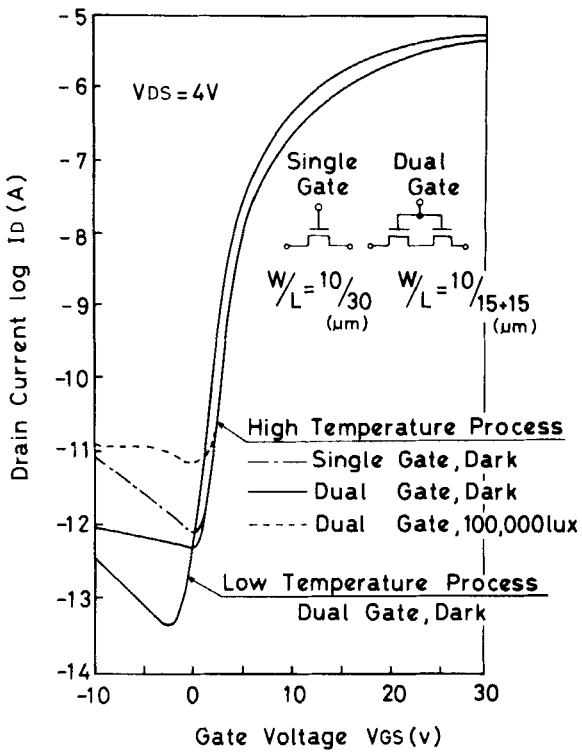

FIGURE 22 Characteristics of poly-Si TFT. The dual reduces the OFF current at the reversed gate bias voltage.

current at high reverse gate bias voltage, the dual gate method is employed. Such leakage current flows through the reversely biased pn junction formed by the *n* type drain electrode and the p type accumulation layer created by the reverse gate voltage. This is because the level of this leakage current increases expoentially with the applied voltage across the junction. If such applied voltage is halved with the dual gate method, the leakage current decreases considerably, as shown in Figure 22. Since the poly-Si film, unlike amorphous silicon film, is not very sensitive to light, the leakage current induced by the 100,000 lux illumination is only 10 pA without light shielding.

The LCD structure with poly-Si TFT array is quite similar to that of a-Si TFT-LCD as shown in Figure 17. On the lower glass substrate, the dual gate poly-Si TFTs and the related ITO pixel electrodes are fabricated. A black stripe metal layer is formed under the color filter layer instead of the black dye area as shown in Figure 17. The TN mode liquid crystal has crossed axes polarizers positioned on both outer sides of the cell. A photograph of the pocket television set incorporating poly-Si TFT array is shown in Figure 23. 220 (V) $\times$ 320 (H) pixels are arranged in a 2″ diagonal area. The contrast ratio of 30:1, and a viewing angle of 45° right and left, and 20°/30° upper and lower over a contrast ratio 10:1 have been obtained. The column driver of "pixel-at-a-time" method, which excludes the analog line memory from the "line-at-a-time" driver as shown in Figure 19, was used. As the ON current of poly-Si TFT is high enough, it does not need to be driven during a full scanning period as in the case of "line-at-a-time" driving. Consequently, the driver circuits are extremely simplified.

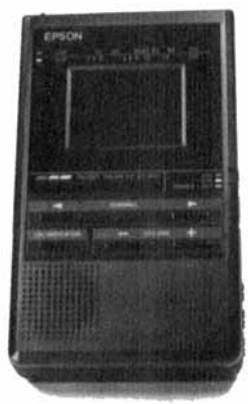

FIGURE 23 Photograph of color TV set with 2″ poly-Si TFT-LCD.

3.2.3. Active matrix LC-TV thin-film diode array. Thin-film diodes for active elements in the active matrix liquid crystal display have been investigated[85] as alternative devices for TFTs. TFTs, after all, require complicated fabrication processes, and some types exhibit instability due to unstable states inside the gate insulator, and in the interface between the gate insulator and semiconductor film. Generally, diodes have relatively stable electrical characteristics and can be fabricated with a simpler process than TFTs. However, in order to obtain a satisfactory active matrix display panel, thin-film diodes must have a steep transient and appropriate threshold voltage as discussed in Section 2.2.2.

Usually, diode elements for active matrix LCDs are fabricated on the glass substrate at relatively low temperature to allow the use of glass material. Figure 24 shows the panel configuration of the diode type active matrix LCD. On the upper glass substrate, a stripe-shaped scanning electrode is formed as for multiplexed TN-LCDs. On the lower substrate, the pixel electrodes are connected to the common data lines through the bidirectional thin-film diode. The color filter layer with the color pixels is normally fabricated on the upper substrate. Although the most suitable driving scheme for diode type active matrix LCD depends on the thin-film diode characteristics,

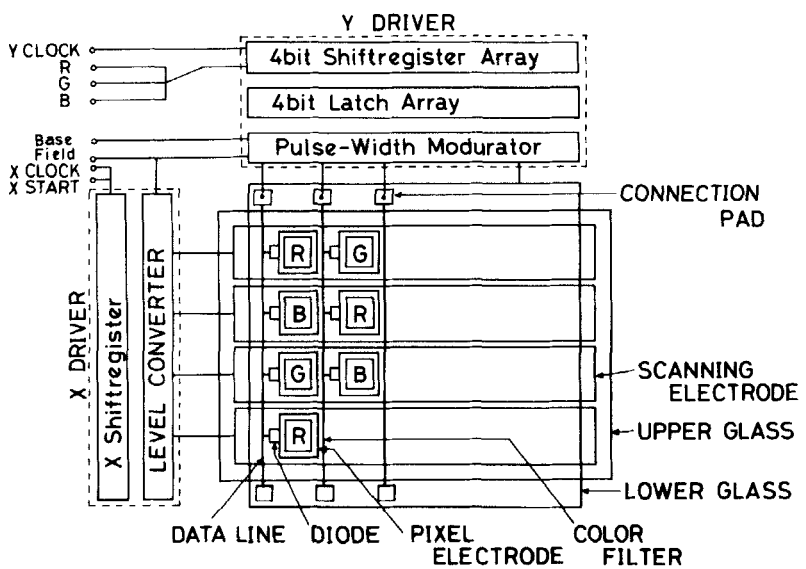

FIGURE 24 Configuration of diode-type active matrix LCD. In this example, gray scales are achieved by pulse-width modulation.

mostly, it is similar to that used in the multiplexed TN method. As for gray scale capability, both the pulse-width modulation as used in the multiplexed TN, and the voltage level application as utilized in the TFT type active matrix LCD, can be used. This figure shows the pulse-width modulation method.

Conventionally, thin-film diodes include a-Si ring diodes,[45] back-to-back connected a-Si diodes,[46] and metal–insulator–metal (MIM) structures[52] featuring electron conduction via traps inside the insulator. Ring diodes have a parallel connection between the forward and reverse a-Si pn diodes, and current characteristics are determined by the forward characteristics of the pn junction. The forward characteristics feature a steep transient, while the forward voltage V_{DI} is only 0.6 volts, and hence the highest voltage applied to the pixel is limited by inequality (17). In order to improve this drawback, the diode connection has been stacked, but this sacrifices steepness. In the back-to-back diode, a couple of reversely disposed diodes are serially connected to have a threshold voltage determined by the breakdown, but such threshold may have an instability problem. A MIM structure with tantalum–tantalum pentoxide–chromium (Ta-Ta_2O_5-Cr) layers, and chromium–silicon nitride–ITO layers[86] have been developed. The Ta-Ta_2O_5-Cr diode, in particular, can be easily fabricated with well-controlled and stable characteristics. However, since the dielectric constant of the Ta_2O_5 film is too large, as much as 25, the parasitic capacitance problem as shown in Section 2.2.2. arises. In order to reduce this capacitance, the lateral structure[53] with only a sidewall is used for conduction, otherwise device dimensions are kept small.

The MIM diode structure with Ta-Ta_2O_5-Cr layers is illustrated in Figure 25. On the glass substrate, Ta film is sputtered and patterned to form the data line and one terminal of the MIM diode, then the

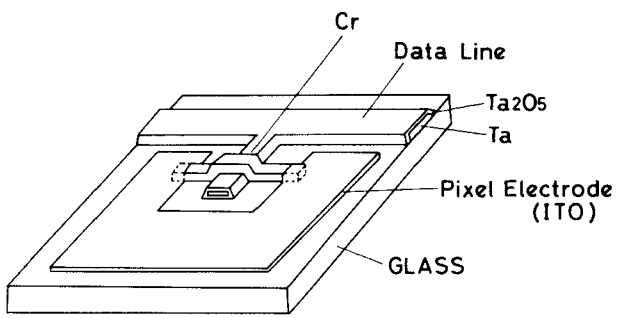

FIGURE 25 Structure of metal-insulator-metal (MIM) diode.

surface of the Ta film is anodic oxidized in 0.01 wt% citric acid solution with DC bias voltage to create a 400–500 Å Ta_2O_5 film. The chromium layer is evaporated and etched off, except for the counter electrode area on the MIM diode, and an ITO film is sputtered to make the pixel electrode. The parasitic capacitance for a small size pixel (e.g. 0.1–0.2 mm square) requires a MIM dimension of 5–10 μm. The breakdown voltage of the MIM diode with Ta_2O_5 thickness of 400 Å is over 20 volts. This diode is fabricated with three photomasks,[80] but if a very thin chromium layer under the ITO film is employed to obtain transparency, the diode can be completed with two photomasks since both films can be deposited and patterned at the same time. Besides, as Ta_2O_5 film is insensitive to light, there is no light shield problem for the TFTs.

The characteristics of MIM diodes are determined by the trap density distribution and by the interface between the Ta_2O_5 and chromium layer. The hetero-interface between the Ta and Ta_2O_5 is considered to be stable due to anodic oxidation (which is not a deposited film), and the inner Ta_2O_5 film is well controlled by the bias voltage during oxidation. As a result, the MIM diode characteristics are highly reliable as long as the Ta_2O_5-Cr interface is clean. Typical characteristics of the MIM are shown in Figure 26. As seen from this figure, current flow in both polarities has good symmetry and the transient is relatively steep.

The MIM diode array mentioned above is applied to the actual liquid crystal display which has 220 × 256 pixels in a 39.6 mm × 52.4 mm display area (2.6″ diagonal), and 220 × 320 pixels in a 50.6 × 67.1 area (3.3″ diagonal). These LCDs use parellel polarizers of TN mode, and obtained a peak contrast ratio of 30:1. A viewing angle of 30°/20° upper/lower, and 45° right/left, over a contrast ratio of 8:1, was realized. The 5 μm × 5 μm MIM diode array is fabricated with three photomasks. A photograph of a pocket-television set with this display is shown is Figure 27. Here, gray scale reproduction is achieved with the pulse-width modulation method.[87] In order to avoid the cross-talk problem due to relatively low ON/OFF current ratio compared to TFTs, polarity of the applied signals to the liquid crystal material is inverted in every double scanning line as mentioned in Section 2.2.2.

3.4. Projection TV with liquid crystal light valves

A projection display, in which a large-scale image can be easily obtained by magnifying an image on the small area, is a realistic way

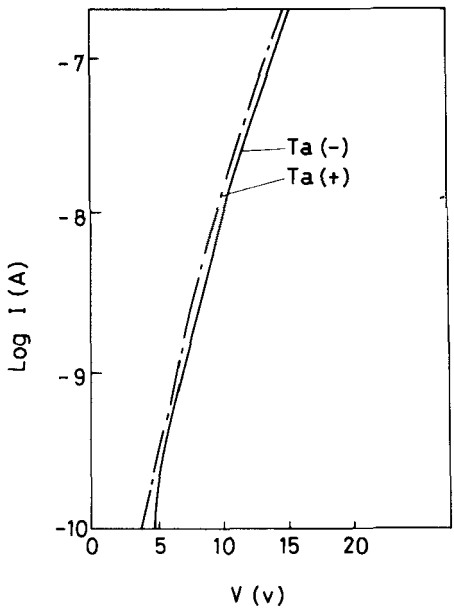

FIGURE 26 MIM Characteristics of Ta-Ta_2O_5-Cr. This structure exhibits good symmetry.

to realize a large display, aside from the direct viewing method. In the case of the liquid crystal display panel, it is quite difficult to make a very large video display over 14″ diagonal. On the other hand, the projection method, with the advantage of a liquid crystal panel controlling the incident light transmission, offers the possibility of a large area and bright screen.

FIGURE 27 Photograph of 2.6″ color TV set with MIM diode array.

Many efforts have been made towards projection displays with liquid crystal light valves primarily addressed by CRTs[88] and laser beams.[89–92] They have been aiming at generating a large, high-resolution screen, but because they use laser-beam thermal addressing to control the scattering effect of smectic mode, they are not applicable to moving pictures such as video. Recently, with the advance of active matrix technology, highly dense pixels in a small area incorporating active elements to create a high image quality have become available for light valves in projection video displays. Initially, this was tried with three 220 (H) × 320 (V) pixel liquid crystal cells in 1.27″ diagonal area, generating a full color image by the synthesis of red, green and blue beams assigned to three light valves.[93] Then, resolution was improved with 440 (V) × 480 (H) pixels,[65] satisfying the full NTSC (National Television System Committee) resolution standards.

The configuration of the full color video projector with three small-sized liquid crystal light valves is shown in Figure 28. The light flux generated by the lamp is transmitted to the light guide through an interference filter, excluding ultraviolet and infrared rays. The beam splitter located in the light guide separates the white light into red, green, and blue beams with a dichroic mirror. Three beams pass the corresponding liquid crystal light valve and are then gathered by the dichroic prism into one beam. Here, the red, green and blue images are synthesized and projected onto the screen through a projection lens. In order to obtain a bright, high quality screen image, the light

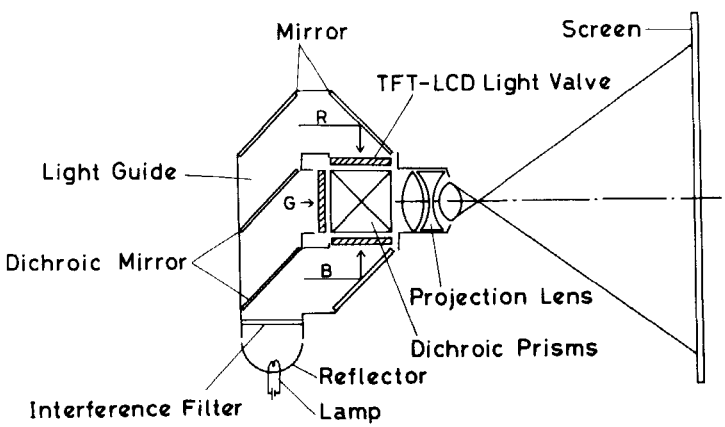

FIGURE 28 Configuration of projection TV with three liquid crystal light valves.

source must have high color temperature, high light conversion efficiency, and long term stability. Among the many kinds of light sources, halogen, xenon, or metal-halide lamps were chosen. Since there is a considerable light loss at the light valves and light guide, a large light flux may be needed for a very bright screen. Usually, around 10,000 lumens total flux at the source is obtained with a 300-watt lamp, in which case a flux of about 100–300 lumens may be projected onto the screen.

The conventional projector with three CRTs inside has large and complicated optics, which may limit brightness, and increase weight and volume. The liquid crystal obviously has a high potential for small, light weight projectors. A smaller liquid crystal panel can realize a smaller and lighter projector, due to the use of a small lens, mirrors, and prism. As for the light valve, poly-Si TFT-addressed active matrix liquid crystal display panels are used. Poly-Si TFT is quite resistant to intense light, and because of the high ON current of poly-Si TFTs, the pixel size can be minimized with smaller TFT devices. Moreover, the driver circuit can be integrated by TFTs if pixel pitch is too small to connect the driver circuits from outside. The poly-Si TFT addressed light valves with 220 × 320 pixels have a pixel size of 90 μm × 80 μm in a 19.8 mm × 25.6 mm active area, and all integrated driver circuits on the same substrate by poly-Si TFTs. Here, an aperture ratio of 70% was obtained. On the other hand, 440 × 480 light valves have a pixel pitch of 65 μm × 80 μm in a 28.6 mm × 38.4 mm active area. This LC light valve has an integrated row driver and its aperture ratio is about 50%.

A full-color video projection display with poly-Si TFT addressed 440 × 480 pixel light valves designed as outlined above exhibited an excellent image quality. With the 300-watt xenon lamp, a screen brightness of 300 ft-lambert on a 6-gain screen of 40″ diagonal was obtained. Although the original contrast ratio at the light valve itself was 100:1, the contrast ratio on the obtained image was degraded to 50:1 due to undesired light scattering inside the optical instruments. The photograph in Figure 29 shows the actual image on the 40″ screen. The obtained resolution was 350 TV lines for the horizontal direction, which is sufficient for the ordinary NTSC standard video signal. Due to the single lens projection method, the screen size and the distance between the lens and the screen can be varied, for the optimum image to meet the environmental requirement when used as a rear projector. The set is about 30 cm × 20 cm × 10 cm, and weighs only 4.5 kg. This makes it very convenient as a portable video projector, as well as for computer graphics.

FIGURE 29 Photograph of image projected onto 40″ screen.

4. LC-TVs IN THE FUTURE

This paper has discussed principles, driving methods, actual performances, and applications of existing liquid crystal display technologies to full color video image reproduction. Figure 30 shows chromaticity diagram of the liquid crystal full color display with the two methods previously discussed: active matrix and highly multiplexed direct-driving TN. The active matrix technology, with active elements such as thin-film transistors or thin-film diodes at each pixel for an extrinsic pixel memory, features an excellent color image, close to CRTs as shown in Figure 30. However, due to complication in fabricating the active elements, it is expensive and difficult to produce with a large area. The area of currently available displays, excluding R & D models, is still only 2″–3″ diagonal. On the other hand, although the image quality (contrast ratio and viewing angle) is not sufficient for practical use, the highly multiplexed direct-driving liquid crystal video display utilizing the TN mode has a simpler fabrication process.

Future LC-TVs will definitely require larger size than the existing panels. As the liquid crystal video display size becomes larger, a much higher image quality, *i.e.* higher contrast ratio, wider viewing angle, higher color purity, more natural gray scale reproduction and higher resolution, equivalent to those of CRTs, will be required. Image

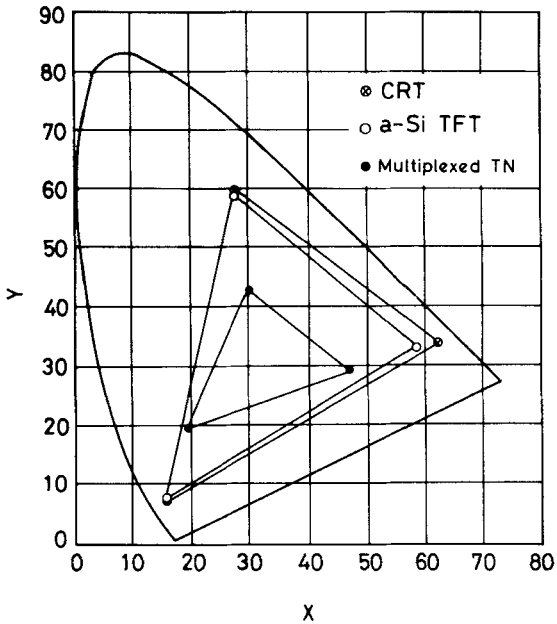

FIGURE 30 Chromaticity diagram of typical full-color liquid-crystal displays incorporated into LC-TVs with multiplexed TN and a-Si TFT active matrix method.[75]

quality and/or response speed of multiplexed direct-driving TN or STN displays is limited by its principles. Although future improvements are expected as discussed in Section 2.1.2., it is unclear whether this approach will satisfy the above requirement. Other direct-driving principles such as ferroelectric liquid crystal[94] has been developed but at the present time it is also unknown whether or not this material is applicable to video displays from the view point of controllability and stability of homogeneous molecular alignment, gray scale capability and response speed. The active matrix may satisfy such image quality requirement with the existing liquid crystal technologies.

The enlargement of the display in the active matrix approach will be a more serious problem than with the multiplexed direct driving type, because of possibly high production costs due to the difficulty of large area fabrication of the active elements on the glass substrate. Such active elements, whose number may be over 1,000,000, have very small dimensions and must be formed on the large area glass substrate with few defects. Defects of active elements and on row and column metallization lines may pose a yield problem. In order to solve this problem, redundancy methods[95] in which additional ac-

tive elements replace the defective elements, have been tried for large area displays such as 12″–14″. The productivity of the glass substrate with active elements may be another problem, because it may determine the production cost as well as production yield. The present active matrix elements are fabricated with production equipments and environment similar to LSIs in order to obtain high yield. However, such production requires a large investment, in spite of its low productivity throughput. Therefore, large area fabrication of the active elements, with high yield and throughput, may be a key factor in the success of a large size liquid crystal video display.

In order to achieve a large area display with excellent color image, a simplified active element fabrication process is needed. This may be achieved using simpler structures with fewer photomasks. The diode structure, rather than TFTs, may have a high potential. Efforts to realize large area and high image quality liquid crystal displays will continue for more than 5 years, assuming promising technologies other than the active matrix approach will not arise. With such efforts, a "wall-hanging" home TV with liquid crystal display of more than 20″ diagonal size, full resolution of NTSC, SECAM or PAL, and color image equivalent to CRTs, may be developed within 5 years. However currently it is not clear whether the active matrix liquid crystal video display will meet the HDTV (high definition television) requirements, i.e. more than 1,000 line resolution and over 40″ in size. Although it is difficult to give a clear forecast of how this technology will fare in the competition with CRTs, LC-TVs will undoubtedly expand their application field and market opportunity to those of CRTs.

5. Acknowledgment

The authors wish to thank Dr. M. M. Labes, Temple University, and Dr. Shunsuke Kobayashi, Tokyo University of Agriculture and Technology, for their encouragement to write this article.

References

1. G. H. Heilmeier, L. A. Zanoni and L. A. Barton, *Proc. IEEE*, **56**, 1162 (1968).
2. J. A. van Raalte, *Proc. IEEE*, **56**, 2146 (1968).
3. A. R. Kmetz in: "Nonemissive Electrooptic Display," edited by A. R. Kmetz and F. V. von Willisen (Plenum, N. Y., 1976), p. 261: SID Seminar Lecture Note, p. 4-1 (1983).
4. T. J. Scheffer, SID Seminar Lecture Note, p. 7. 1-2 (1986).

5. A. I. Lakatos: *IEEE Trans. Electron Devices*, ED-30, 525 (1983).
6. W. E. Howard, Seminar Lecture Notes of SID, **7**, 2 (1986).
7. A. Sasaki and T. Uchida, *Proc. International Display Research Conference*, **3**, 1 (1986).
8. S. Morozumi, K. Oguchi and H. Ohshima, *Optical Engineering*, **23**, 241 (1984).
9. M. Schadt and W. Helflich: *Appl. Phys. Lett.*, **18**, 127 (1971).
10. P. M. Alt and P. Pleshko, *IEEE Trans.*, **FD-21**, 146 (1974).
11. E. Kaneko, H. Kawakami and H. Hanmura, *Proc. SID*, **19**, 55 (1978).
12. G. Bauer in : "The Physics and Chemistry of Liquid Crystal Devices," edited by G. J. Sprokel (Plenum, N.Y., 1980), p. 61.
13. C. Z. von Doarn, C. J. Gerritsma and J. J. M. J. de Klerk, *ibid*, p. 95.
14. Birecki and F. J. Kahn, *ibid*, p. 125.
15. M. Schadt and P. R. Gerber, *Z. Naturforsh*, **37a**, 165 (1982).
16. T. Uchida, *Mol. Cryst. Liq. Cryst.*, **123**, 15 (1985).
17. E. Kaneko, H. Kawakami and H. Hanmura, *SID Symp. Digest*, 92 (1978).
18. E. Kaneko, H. Hanmura, H. Kawakami and S. Sato, *SID Symp. Digest*, 84 (1981).
19. H. Ideno and H. Arai, *Technical Report of IEICE Japan*, EID86- 22, 25 (1986).
20. K. Kinugawa, Y. Kando and M. Kanasaki, *SID Symp. Digest*, 122 (1986).
21. T. J. Scheffer and J. Nehring, *J. Appl. Phys.*, **58**, 3022 (1985).
22. M. Schadt and F. Leenhouts, *Appl. Phys. Lett.*, **50**, 236 (1987).
23. K. Kawasaki, K. Yamada, R. Watanabe and K. Mizunoya, *SID Symp. Digest*, 391 (1987).
24. M. Nagata, H. Wada, C. Ijima, S. Wada, O. Okumura, R. Miyazaki, Y. Iwashita and H. Takeshita, National Conf. Record, 1987 *Semic. Dev. Materials IEICE*, Japan, 1–289 (1987).
25. B. J. Lechner, F. J. Marlowe, E. O. Nester and J. Tults, 1969 *International Solid State Circuits Conference*, Digest of Technical Papers, 52 (1969).
26. B. J. Lechner, F. J. Marlowe, E. O. Nester and J. Tults, *Proc. IEEE.*, **59**, 1566 (1971).
27. P. K. Weimer, G. Sadasiv, L. Meray-Horvath and W. S. Homa, *Proc. IEEE.*, **53**, 354 (1966).
28. A. G. Fischer, *IEEE. Trans. Electron Devices*, **ED-18**, 802 (1971).
29. T. P. Brody, J. A. Asars and G. D. Dixon, *IEEE Trans.*, **ED-31**, 995 (1973).
30. T. P. Brody, J. A. Asars and G. D. Dixon, *SID Symp. Digest*, 179 (1973).
31. L. T. Lipton and N. J. Koda, *Proc. SID*, **14**, 127 (1973).
32. F. C. Luo and W. A. Hester, *IEEE. Trans. Electron Devices*, **ED-27**, 223 (1980).
33. M. J. Lee, S. W. Wright and C. P. Judge, *Proc. SID*, **23**, 37 (1982).
34. F. C. Luo, J. Patterson, T. Braunstein and D. Leksell, *SID Symp. Digest*, 286 (1985).
35. L. T. Lipton, C. P. Stephens and R. B. Lloyd, *SID Symp. Digest*, 65 (1977).
36. L. T. Lipton, M. A. Meyer and D. O. Massetti, *SID Symp. Digest*, 78 (1975).
37. M. Matsuura, Y. Takafuji, K. Nonomura, F. Funada and T. Wada, *SID Symp. Digest*, 148 (1983).
38. M. Yoshiyama, T. Matsuo, K. Kawasaki, H. Tatsuta and T. Ishihara, *Mol. Cryst. Liq. Cryst.*, **68**, 1195 (1981).
39. M. Hosokawa, K. Oguchi, M. Ikeda, S. Yazawa and K. Endo, *SID Symp. Digest*, 114 (1981).
40. W. E. Spear and P. G. LeComber, *Solid-State Commun.*, **17**, 1193 (1975).
41. S. Morozumi, K. Oguchi, S. Yazawa, T. Kodaira, H. Ohshima and T. Mano, *SID Symp. Digest*, 156 (1983).
42. T. P. Brody, *IEEE. Trans. Electron Devices*, **ED-31**, 1614 (1984).
43. D. E. Castleberry, *Proc. SID*, **20**, 197 (1979).
44. D. R. Baraff, J. R. Long, B. K. MacLaurin, C. J. Miner and R. W. Streater, Biennial Display Research Conference, 107 (1980).
45. S. Togashi, K. Sekiguchi, H. Tanabe, E. Yamamoto, K. Sorimochi, E. Tajima, H. Watanabe and H. Shimizu, *Proc. SID*, **26**, 9 (1985).

46. N. Szydlo, E. Chartier, J. N. Perbert, N. Proust, J. Magarinor and M. Hareng, *Proc. Japan Display*, 416 (1983).
47. K. Niwa, S. Maezawa, M. Suzuki, T. Takeuchi and T. Kamikawa, *SID Symp. Digest*, 304 (1984).
48. S. Togashi, K. Sekiguchi, H. Tanabe, T. Okigami, M. Okamoto, K. Sorimachi, E. Yamamoto, O. Sugiyama, N. Taguchi, S. Ishimori, M. Kikuchi, A. Suzuki, E. Tajima and T. Aoyama, *Proc. Japan Display*, **PD-4**, (1986).
49. T. Katagishi, Y. Marushita, Y. Okita, M. Yamashita and H. Takesada, *SID Symp. Digest*, 285 (1986).
50. Y. Nasu, S. Kawai, S. Kisumi, K. Oki and K. Hori, *SID Symp. Digest*, 289 (1986).
51. P. Migliorato, *Proc. Eurodisplay*, 44 (1987).
52. D. R. Baraff, J. R. Long, B. K. MacLaurin, C. J. Miner and W. Streater, *IEEE Trans.*, **ED-28**, 736 (1981).
53. S. Morozumi, T. Ohta, R. Araki, T. Sonehara, K. Kubota, Y. Ono, T. Nakagawa and H. Ohara, *Proc. Japan Display*, 404 (1983).
54. C. H. Gooch and H. A. Tarry, *J. Phys., D*, **8**, 1575 (1975).
55. S. Nagata, T. Ogawa, K. Adachi, S. Hotta and M. Yoshiyama, *SID Symp. Digest*, 84 (1985).
56. F. Funada, M. Okada, N. Kimura S. Kozaki and K. Awane, *Technical Paper of Inst. Elec. Inf. Commun. Eng. Japan*, **87**, 19 (1988).
57. T. Unate, Y. Matsushita, Y. Ugai and S. Aoki, *Technical Paper of Inst. Elec. Inf. Commun. Eng. Japan*, **87**, 13 (1988).
58. Y. Ugai, Y. Murakami, J. Tamamura and S. Aoki, *SID Symp. Digest*, 308 (1984).
59. J. F. Clerc and J. C. Deutsch, *Proc. Eurodisplay*, 111 (1987).
60. M. F. Shiekel and K. Fahrenschon, *Appl. Phys. Lett.*, **19**, 391 (1971).
61. T. Uchida, *Optical Eng.*, **23**, 247 (1984).
62. T. Uchida, *Proc. Eurodisplay*, 39 (1981).
63. T. Uchida, S. Yamamoto and Y. Shibata, Conf. Rec. of Int'l Display Res. Conf., p. 166 (1982): *IEEE Trans.* **ED-30**, 503 (1983).
64. H. Hasebe and S. Kobayashi, *SID Symp. Digest*, 81 (1985).
65. S. Aruga, R. Araki, H. Kamakura, J. Shinozaki and S. Morozumi, *SID Symp. Digest*, 75 (1987).
66. A. G. Fischer, T. P. Brody and W. S. Escott, IEEE Conf. Rec. of 1972 Conf. on Display Devices, p. 64 (1972).
67. H. Suginoya, H. Kamamori, Y. Terada, N. Kato and K. Iwasa, *Proc. Japan Display*, 206 (1983).
68. H. Watanabe, S. Hashimoto, M. Yoshida, H. Shimizu, A. Tsuzuki and S. Morokawa, *SID Symp. Digest*, 86 (1985).
69. W. J. Latham, T. L. Brewer, D. W. Hawley, J. E. Lamb III and L. K. Stichinote, *SID Symp. Digest*, 379 (1987).
70. D. A. Bolon, V. J. Eddy, P. J. Codella and J. E. Hallgren, *ibid*, 395 (1987).
71. P. G. LeComber, W. E. Spear and A. Ghaith, *Electronics Letters*, **15**, 179 (1979).
72. Y. Okubo, T. Nakagiri, Y. Osada, M. Sugata, N. Kitahara and K. Hatanaka, *SID Symp. Digest*, 40 (1982).
73. S. Kawai, N. Takagi, T. Kodama, K. Asama and S. Yanagisawa, *SID Symp. Digest*, 42 (1982).
74. M. J. Powell, *Appl. Phys. Lett.*, **43**, 597 (1983).
75. S. Hotta, S. Nagata, Y. Miyata, K. Yokoyama, K. Adachi, T. Chikamura, M. Yoshiyama A. Nishikawa and K. Kawasaki, *SID Symp. Digest*, 296 (1986).
76. T. Yanagisawa, K. Kasahara, Y. Okada, K. Sakai, Y. Komatsubara, I. Fukui, N. Mukai, K. Ide, S. Matsumoto and H. Hori, *Proc. SID*, **26**, 213 (1985).
77. D. G. Ast, Conference Record of 1982 International Display Research Conference, 152 (1982).
78. M. J. Powell, J. A. Chapman and M. V. C. Stroomer, *Proc. SID*, **25**, 269 (1984).
79. T. I. Kamins, *Solid State Electronics*, **15**, 789 (1972).

80. S. Morozumi, Conference Rec. of International Display Research Conference, 9 (1985).
81. J. R. Troxell, M. I. Harrington, J. C. Erskine, E. H. Dumbaugh, F. P. Fehlner and R. A. Miller, *IEEE Electron Device Letters*, **ED-7**, 597 (1986).
82. S. Morozumi, R. Araki, H. Ohshima, M. Matsuo, T. Nakazawa and T. Sato, *Proc. Japan Display*, 196 (1986).
83. M. Matsui, Y. Shiraki, Y. Katayama, K. Kobayashi, A. Shintani and E. Maruyama, *Appl. Phys. Lett.*, **37**, 936 (1980).
84. Y. Oana, *SID Symp. Digest*, 312 (1984).
85. W. E. Howard, *Proc. SID*, **27**, 313 (1986).
86. M. Suzuki, M. Toyama, T. Harajiri, T. Maeda and T. Yamazaki, *Proc. Japan Display*, 72 (1986).
87. S. Maezawa, S. Yazawa, K. Niwa, T. Ushiki, T. Takano, Y. Wakai, H. Baba, M. Suzuki and K. Koide, *SID Symp. Digest*, 54 (1987).
88. W. P. Bleha, J. Grinberg and A. D. Jacobson, *SID Symp. Digest*, 42 (1973).
89. F. J. Kahn, *Appl. Phys. Lett.*, **22**, 111 (1973).
90. K. Kubota, S. Sugama, S. Naemura and N. Nishida, *SID Symp. Digest*, 44 (1983).
91. F. J. Kahn, P. N. Kendrick, J. Leff, L. J. Livoni, B. E. Loucks and D. Stepner, *SID Symp. Digest*, 254 (1987).
92. Y. Nagae, E. Kaneko, Y. Mori, and H. Kawakami, *SID Symp. Digest*, 368 (1986).
93. S. Morozumi, T. Sonehara, H. Kamakura, T. Ono and S. Aruga, *SID Symp. Digest*, 375 (1986).
94. N. A. Clark and S. T. Langerwall, *Appl. Phys. Lett.*, **36**, 899 (1980).
95. M. Takeda, S. Ogo, T. Tamura, H. Kamiura, H. Noda, T. Kawaguchi, I. Yamashita, D. Ando and H. Kuroda, *Proc. Japan Display*, 204 (1986).